Robust estimation of lumbar joint forces in symmetric and asymmetric lifting tasks via large-scale electromyography-driven musculoskeletal models

Moya-Esteban, A.; van der Kooij, H.; Sartori, M.

Important note
To cite this publication, please use the final published version (if applicable).
Please check the document version above.

Check for updates

Robust estimation of lumbar joint forces in symmetric and asymmetric lifting tasks via large-scale electromyography-driven musculoskeletal models

A. Moya-Esteban [a,*], H. van der Kooij [a,b], M. Sartori [a]

[a] *Department of Biomechanical Engineering, University of Twente, Enschede, The Netherlands*
[b] *Department of Biomechanical Engineering, Delft University of Technology, Delft, The Netherlands*

ARTICLE INFO

ABSTRACT

Low back joint compression forces have been linked to the development of chronic back pain. Back-support exoskeletons controllers based on low back compression force estimates could potentially reduce the incidence of chronic pain. However, progress has been hampered by the lack of robust and accurate methods for compression force estimation. Electromyography (EMG)-driven musculoskeletal models have been proposed to estimate lumbar compression forces. Nonetheless, they commonly underrepresented trunk musculoskeletal geometries or activation–contraction dynamics, preventing validation across large sets of conditions. Here, we develop and validate a subject-specific large-scale (238 muscle–tendon units) EMG-driven musculoskeletal model for the estimation of lumbosacral moments and compression forces, under eight box-lifting conditions. Ten participants performed symmetric and asymmetric box liftings under 5 and 15 kg weight conditions. EMG-driven model-based estimates of L5/S1 flexion–extension moments displayed high correlation, R^2 (mean range: 0.88–0.94), and root mean squared errors between 0.21 and 0.38 Nm/kg, with respect to reference inverse dynamics moments. Model-derived muscle forces were utilized to compute lumbosacral compression forces, which reached eight times participants body weight in 15 kg liftings. For conditions involving stooped postures, model-based analyses revealed a predominant decrease in peak lumbar EMG amplitude during the lowering phase of liftings, which did not translate into a decrease in muscle–tendon forces. During eccentric contraction (box-lowering), our model employed the muscle force–velocity relationship to preserve muscle force despite significant EMG reduction. Our modeling methodology can inherently account for EMG-to-force non-linearities across subjects and lifting conditions, a crucial requirement for robust real-time control of back-support exoskeletons.

1. Introduction

Low back pain (LBP) is a common musculoskeletal disorders worldwide *i.e.*, 84% of the population is expected to experience it at some point in time (Balagué et al., 2012). Excessive low back joint compression forces have been identified as a major risk for the development of chronic LBP (Coenen et al., 2013, 2014). Prolonged handling of heavy objects or repeated lifting tasks are physically demanding activities, with high incidence within occupational domains, which underlie large lumbar compression forces (Ning et al., 2014). On top of its impact on individuals' quality of life, LBP encompasses an economical hardship as a result of medical diagnosis, treatment costs and sick leave (Lambeek et al., 2011).

Robotic exoskeletons could protect musculoskeletal tissues by providing assistive forces that off-load target biological joints. In past years, much attention was paid to occupational scenarios (De Looze et al., 2016), with exoskeletons being adopted in automotive or logistics settings. In this context, back-support exoskeletons aim at relieving the back musculoskeletal system from excessive muscular forces and spinal joint compression forces (Bosch et al., 2016; Huysamen et al., 2018), contributing to reduce the incidence of LBP.

In the context of active back-support exoskeletons, there is no consensus on the optimal control strategy to be employed. Potential solutions include the non-invasive measurement of bioelectrical or biomechanical signals and their subsequent incorporation into device control loops. Controllers were proposed, which aimed at reducing electromyographic (EMG) activity in thoracolumbar muscles (Hara and Sankai, 2010). Nonetheless, due to the highly non-linear relationship between EMG and joint loading (Potvin et al., 2004), a reduction of back muscle EMG activity would not imply an equal reduction in intervertebral joint compression forces. On the contrary, the magnitude of compression forces is directly related to back muscle–tendon

---

* Corresponding author.

E-mail address: a.moyaesteban@utwente.nl (A. Moya-Esteban).

Nomenclature

ρ	Pearson's correlation coefficient
CEINMS	Calibrated EMG-informed Neuromusculoskeletal
EMG	Electromyography
FL	Force–length (relationship)
FV	Force–velocity (relationship)
GRF	Ground reaction forces
ID	Inverse dynamics
IK	Inverse kinematics
LBP	Low back pain
LFB	Lifting full body
LT	Lift transfer
LTpL	Longissimus thoracis pars lumborum
LTpT	Longissimus thoracis pars thoracis
LTT	Left twist transfer
MTU	Muscle–tendon unit
RMSE	Root mean squared error
$RMSE_{BW}$	Root mean squared error normalized to body weight
$RMSE_{RMS}$	Root mean squared error normalized to root mean square of the reference moment
RTT	Right twist transfer
SQ	Squat
ST	Stoop
TT	Twist transfer

forces (Koopman et al., 2020a, 2019). Therefore, an exoskeletal technology controlled as a direct function of an individual's lumbar joint compression forces would have the potential for controlling a key factor underlying LBP and related injuries.

Fundamental requirements for the development of such control technology are estimation accuracy and robustness, *i.e.* the ability to estimate accurate back muscle forces and resulting joint compression forces in large sets of conditions. Modeling approaches relying on static optimization which typically minimize muscle stress (Bazrgari et al., 2007; van Dieën and Kingma, 1999) or activation (von Arx et al., 2021; Kim and Zhang, 2017) have been proposed for the estimation of lumbar muscle and compression forces in healthy participants performing symmetric and asymmetric squat and stooped liftings. However, these methodologies neglect antagonistic co-contraction (Hughes et al., 1995), which may entail reduced estimation accuracy. Moreover, although a chosen objective function may be suitable to estimate multi-muscle activation in a specific motor task, this may not necessarily generalize to biomechanically different tasks. Alternatively, accuracy and robustness may be achieved with the development of an experimental and computational framework that takes into account the anatomy and neuromechanics of thoracolumbar musculature for a specific individual. That is, large-scale 3D musculoskeletal geometry, muscle activation and contraction dynamics. This could be achieved by combining EMG measurements with signal-driven musculoskeletal modeling approaches (Lloyd and Besier, 2003; Sartori et al., 2012; Gerus et al., 2013).

EMG-driven musculoskeletal models were previously proposed for the estimation of lumbar moments and compression forces. However, these were only assessed under a limited set of weight and lifting conditions (Cholewicki et al., 1995; Sparto et al., 1998), relied on limited representations of thoracolumbar musculoskeletal geometry (*e.g.*, reduced number of muscle–tendon units with simplified lines of actions and moment arms) (Hughes et al., 1994; Ning et al., 2012), or included simplified representations of muscle activation and contraction dynamics (Nussbaum and Chaffin, 1998; van Dieën and Kingma, 2005;

Marras and Granata, 1997). Hence, the robustness of these models for real-world scenarios underlying diverse movements and loads may be compromised.

Here, we developed and validated a large-scale (238 muscle–tendon units), physiologically correct, EMG-driven musculoskeletal model of the trunk. For ten healthy individuals, we identified a single set of muscle–tendon unit parameters per person, which produced valid estimates of lumbosacral moments and realistic compression forces in a repertoire of eight box-lifting conditions including: two symmetric and two asymmetric lifting techniques, and two box weights (5 and 15 kg). Our results also showed the ability of the proposed EMG-driven model to account for the inherent non-linearity between EMGs and musculoskeletal forces *i.e.*, decrease in trunk muscle EMG with no loss in resulting mechanical force, which was prominent in specific phases of the lifting-lowering cycle. Accounting for EMG-to-force non-linearities is crucial for developing robust model-based control paradigms for robotic exoskeletons.

The present study represents the first step towards the development of an accurate and robust EMG-informed model-based framework for the simulation of trunk mechanics and the development of versatile human-exoskeleton interfaces for out-of-lab scenarios.

2. Methods

2.1. Data collection

Experimental procedures were approved by the Natural Sciences and Engineering Sciences Ethics committee of the University of Twente (reference number: 2020.20) and all participants gave written informed consent. Ten male participants (28 $\pm$ 2 years old; body mass: 72 $\pm$ 8 kg; height: 177 $\pm$ 9 cm) without history of low back pain performed box-liftings tasks (Fig. 1).

Symmetric box-lifting conditions: two symmetric lifting techniques were used to lift a box (width $\times$ depth $\times$ height: 40 $\times$ 30 $\times$ 22 cm) placed on a platform (height: 28 cm) in front of participants: squatting (SQ) and stooping (ST). *Asymmetric box-lifting conditions:* two tables (55 $\times$ 55 $\times$ 40 cm) were placed at 60 degrees to the left and right of the subjects' sagittal plane. Two asymmetric lifting techniques were performed, including lift-transfer (LT) and twist-transfer (TT). Participants were instructed to transfer the box unilaterally from the platform to the right table (LT) or from the left to the right table (TT) with stoop-like postures. Subsequently, participants returned the box to the initial position. For each lifting technique, 5 and 15 kg weight conditions were considered.

Subjects completed 40 lifting trials (five trials per experimental condition) and each trial consisted of two repetitions. To prevent muscle fatigue onset, participants rested one minute after each trial. The trial order was randomly pre-allocated to prevent potential order-related confounding effects.

Ground reaction forces (GRF) and EMGs were recorded at 2048 Hz using a dual force plate (AMTI, MA) and Delsys Bagnoli system (Delsys, Boston, MA). Twelve bipolar EMG electrodes were placed bilaterally on each subject's abdominal and lumbar muscles (Table 1). Full-body and box kinematics were recorded using a twelve-camera motion capture system (Qualisys Medical AB, Sweden). The 3D trajectories of 66 spherical reflective markers (58 on the participant and eight on the box) were recorded at 128 Hz. Markers were placed on bony landmarks and on body segments (triplets) as previously described in Moya-Esteban et al. (2020). GRF and marker trajectories were low-pass filtered (cut-off frequency: 6 Hz). To obtain EMG linear envelopes, raw bipolar signals were: bandpass filtered (30–300 Hz), full-wave rectified and low-pass filtered (6 Hz). All filters were zero-lag 2nd order Butterworth filters. EMG linear envelopes were normalized using data from maximum voluntary contraction recordings (performed as described in McGill, 1991). Unless stated otherwise, hereafter the term EMG will refer to normalized EMG linear envelopes.
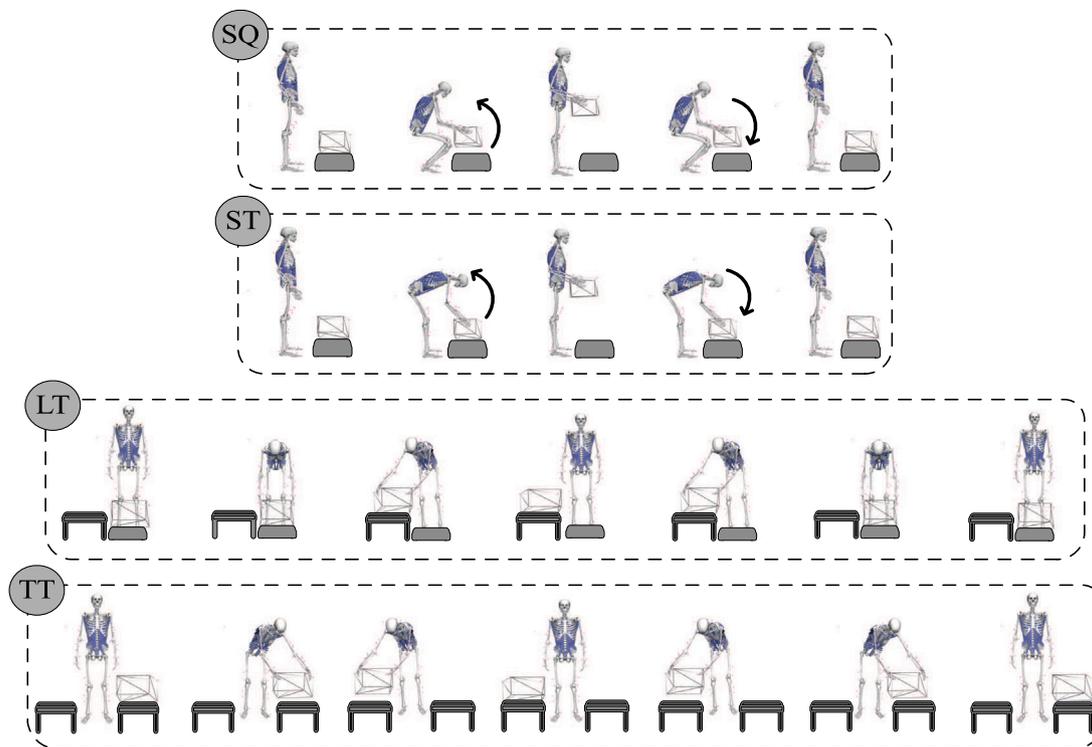
Fig. 1. Movement sequences for symmetric and asymmetric lifting techniques. Each dashed box represent one single repetition for the specific technique, top to bottom: squat (SQ: lifting the box maintaining the trunk as upright as possible while flexing the knees), stoop (ST: lifting the box with extended, but not locked, knees), lift-transfer (LT) and twist-transfer (TT). During symmetric liftings, each repetition involved: (1) bending over to grab the box, (2) lifting the box until upright posture, (3) bending over to place the box and (4) returning to upright posture. For asymmetric liftings, the box was initially placed on the platform (LT) or the left table (TT). Each trial consisted on: (1) stoop to grab the box (either in the sagittal plane in case of LT or leftwards in case of TT), (2) place the box on the right table, (3) returning to upright posture, (4) stoop to grab the box from the right table and (5) transfer it back it to the initial point.

Table 1

Muscle group from which electromyograms (EMGs) were measured and associated muscle–tendon unit (MTU) groups modeled in lifting full body model (LFB). Values within parenthesis indicate the number of modeled MTUs within the group. Bipolar EMG electrodes were placed on: Rectus abdominis (umbilicus level), internal oblique (superior to the inguinal ligament), external oblique muscle (midaxillary line, halfway between the iliac crest and the lowest edge of the rib cage), iliocostalis lumborum (6 cm lateral to L2), longissimus thoracis pars lumborum (3 cm lateral to L1) and pars thoracis (4 cm lateral to T10).

LFB model MTU group	EMG channel
Multifidus (50)	Longissimus thoracis pars lumborum
Longissimus thoracis pars lumborum (10)	Longissimus thoracis pars lumborum
Iliocostalis lumborum pars lumborum (8)	Iliocostalis pars lumborum
Longissimus thoracis pars thoracis (42)	Longissimus thoracis pars thoracis
Iliocostalis lumborum pars thoracis (16)	Longissimus thoracis pars thoracis
Psoas major (22)	Not assigned (passive)
Rectus abdominis (2)	Rectus abdominis
External oblique (12)	External oblique
Internal oblique (12)	Internal oblique
Quadratus lumborum (36)	Not assigned (passive)
Latissimus dorsi (28)	Not assigned (passive)

2.2. Multi-body dynamics modeling

The OpenSim lifting full-body (Beaucage-Gauvreau et al., 2019) geometry model was linearly scaled to match each participant's anthropometry using the recorded 3D marker positions. This geometrical model comprised 238 Hill-type muscle–tendon units (MTUs) representing lumbar, thoracic and abdominal muscles. In this model, net trunk motion was distributed across six intervertebral joints (L5/S1 until T12/L1) using linear kinematic coupling constraints. A separate OpenSim model representing the box (including specific dimensions, weight and inertial properties) was created and used to perform box inverse kinematics (IK) and inverse dynamics (ID) analyses, for each individual lifting trial. Box ID analyses resulted in three rotational moments and three translational forces, which were used to define external hand forces subsequently applied to the middle position between the second and fifth knuckle in the full-body model. Consequently, full-body joint angles, muscle–tendon unit lengths and moment arms were obtained from marker trajectories via IK computation. Finally, joint angles, GRF and external box forces and moments were used to obtain net joint moments via ID. All analyses were performed in OpenSim 4.0 (Delp et al., 2007).

2.3. EMG-driven musculoskeletal modeling

A trunk EMG-driven musculoskeletal model was created using CEINMS toolbox (Calibrated EMG-informed Neuromusculoskeletal), which we previously developed (Pizzolato et al., 2015; Sartori et al., 2012). This relied on the musculoskeletal geometry model detailed in Section 2.2. The developed EMG-driven model enabled estimating net L5/S1 joint moments (hereafter referred as "estimated moments")
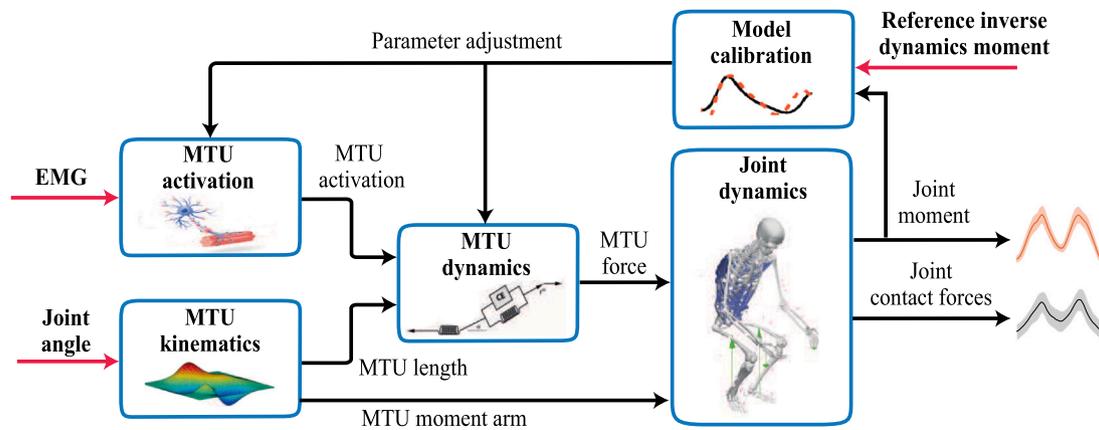
Fig. 2. CEINMS block diagram depicting its five main blocks: muscle–tendon unit (MTU) kinematics, MTU dynamics, MTU activation, joint dynamics and model calibration. The MTU kinematics block utilizes experimental joint angles as input to compute MTU lengths and moment arms. The MTU activation block maps the EMG activity to activations of MTU in the model. The MTU dynamics block computes MTU forces using MTU activation and MTU kinematics as input. The model calibration block calculated physiological MTU parameters (maximum isometric force, tendon slack length and optimal fiber length). Generic initial values were tuned according to predefined boundaries using a simulated annealing algorithm which minimized the summed squared error between reference (inverse dynamics) and estimated joint moments (Goffe et al., 1994) After calibration, the model operated in open-loop using EMG and joint kinematics as input.

as well as underlying muscle–tendon mechanics, using experimentally measured joint angles and EMG as input. Hence, a mapping between measured bipolar EMG channels and MTUs in the full-body model was established (Table 1). Fig. 2 depicts the EMG-driven model major components (Sartori et al., 2012).

For each participant, one subject-specific EMG-driven model was established. Maximal isometric force, tendon slack length and optimal fiber length were calibrated for each of the modeled 238 MTUs, based on EMG, MTU length, MTU moment arms and reference ID moments (Fig. 2). The calibration stage used one random lifting repetition (1 out of 10) from each of the eight experimental conditions to calibrate the aforementioned MTU parameters, yielding to one single calibrated model per participant. The calibrated model was then used to estimate MTU forces and L5/S1 joint flexion–extension moments for the nine remaining repetitions of each experimental conditions, based solely on EMG and joint angles. Finally, estimated MTU forces were projected onto the L5/S1 joint to calculate joint contact forces and moments.

2.4. Study analyses

The first test in this study assessed the validity of our EMG-driven methodology to estimate lumbosacral joint moments. This was assessed by computing the coefficient of determination (R^2) and root mean squared errors (RMSE) between reference ID and estimated moments. The second test analyzed the non-linearity between EMG and MTU force at box-lifting and lowering instances, focusing on the role of muscle force–length and force–velocity relationships.

2.5. EMG-to-force relation

For dorsal muscles (Table 1), maximum EMG peaks at box-lifting and lowering phases were determined as the average over a 100 ms window centered around EMG maxima. The associated MTU forces generated at EMG maxima were derived from our EMG-driven modeling pipeline.

Force contributions from active force–length (FL) and force–velocity (FV) relationships at lifting and lowering instances were extracted from each subject-specific model (Lloyd and Besier, 2003). For each condition and muscle, mean FL-dependent and FV-dependent forces were computed and normalized by maximal isometric force.

2.6. Statistical analyses

Statistical analyses were performed with SPSS software (IBM SPSS Statistics 26, SPSS Corporation, USA). Paired samples t-tests checked for statistical differences between peak EMG (and associated MTU force) at box-lifting and lowering phases, as defined in Section 2.5. First, residuals normality was tested using Shapiro–Wilk tests. Whenever residuals normality was not met, non-parametric Wilcoxon signed-rank tests were used. In case of asymmetric residual distribution, paired-samples sign tests were performed. Statistical significance was accepted at $p < 0.05$.

Pearson's correlation coefficients (ρ) were computed to analyze the relationship between EMG and MTU force. We compared the percent change in EMG at box-lifting and lowering instances, and the percent change in FL-dependent and FV-dependent MTU forces.

3. Results

3.1. Model estimation accuracy

Reference and estimated L5/S1 joint flexion–extension moments for all experimental conditions are shown in Fig. 3. Table 2 and Fig. 4 show a quantitative comparison of lumbar moments and similarity metrics between reference and estimated moments. Histograms in Fig. 4 depict a right-skewed distribution for R^2 and left-skewed for $RMSE_{RMS}$ values (RMSE normalized with respect to the root mean square of the reference moment). Across all participants and conditions, our model estimated L5/S1 joint moments with mean R^2 and $RMSE_{RMS}$ of 0.914 ± 0.03 and 0.198 ± 0.04, respectively.

At lift-off (approximately 25% of the lifting-lowering cycle), the rotational and translational box forces applied to the participants' hands caused the net joint extension moment to experience a peak due to box weight and inertial properties (Fig. 3). For reference moments, the mean peak was approximately 0.3 Nm/kg higher during stoop, lift-transfer and twist-transfer conditions compared with squat, for both 5 and 15 kg conditions (Table 2). Analogous extension moment increments between reference and estimated moments were observed for all participants and experimental conditions, as suggested by mean R^2 (range: 0.88–0.94) and RMSE values (range: 0.21–0.38 Nm/kg).

During symmetric liftings, we observed two peaks in reference and estimated moments: after box lift-off and during box-lowering, just before box placement (Fig. 3). Across symmetric conditions, mean peak magnitudes ranged between 1.78 and 2.33 Nm/kg for estimated

Table 2

Mean L5/S1 estimated and reference peak moments, L5/S1 peak compression forces, coefficient of determination (R^2) and root mean squared errors normalized to body weight ($RMSE_{BW}$) and normalized with respect to the root mean square of the reference moment ($RMSE_{RMS}$). Moments are normalized to body weight (BW) and forces are shown as times body weight. For all conditions, mean values ($\pm$ standard deviation) across all participants are shown. Lifting techniques are squat (SQ), stoop (ST), lift-transfer (LT) and twist-transfer (TT).

	Estimated moment [Nm/kg]	Reference moment [Nm/kg]	L5/S1 Comp. force [xBW]	R^2 [–]	$RMSE_{BW}$ [Nm/kg]	$RMSE_{RMS}$ [–]
SQ 5 kg	1.78 (0.29)	1.65 (0.32)	6.42 (1.42)	0.91 (0.04)	0.21 (0.05)	0.22 (0.04)
SQ 15 kg	2.33 (0.26)	2.37 (0.51)	7.83 (1.10)	0.88 (0.04)	0.30 (0.07)	0.22 (0.04)
ST 5 kg	1.83 (0.39)	1.89 (0.27)	6.30 (1.40)	0.94 (0.02)	0.22 (0.07)	0.20 (0.06)
ST 15 kg	2.30 (0.45)	2.53 (0.38)	7.50 (1.44)	0.92 (0.03)	0.27 (0.06)	0.18 (0.03)
LT 5 kg	1.89 (0.26)	1.84 (0.23)	6.40 (1.17)	0.93 (0.02)	0.21 (0.04)	0.17 (0.03)
LT 15 kg	2.38 (0.35)	2.66 (0.40)	7.72 (1.40)	0.91 (0.02)	0.33 (0.05)	0.20 (0.02)
TT 5 kg	1.82 (0.30)	1.86 (0.23)	6.50 (1.26)	0.92 (0.02)	0.23 (0.06)	0.18 (0.04)
TT 15 kg	2.33 (0.38)	2.65 (0.39)	7.71 (1.19)	0.91 (0.04)	0.38 (0.07)	0.21 (0.03)
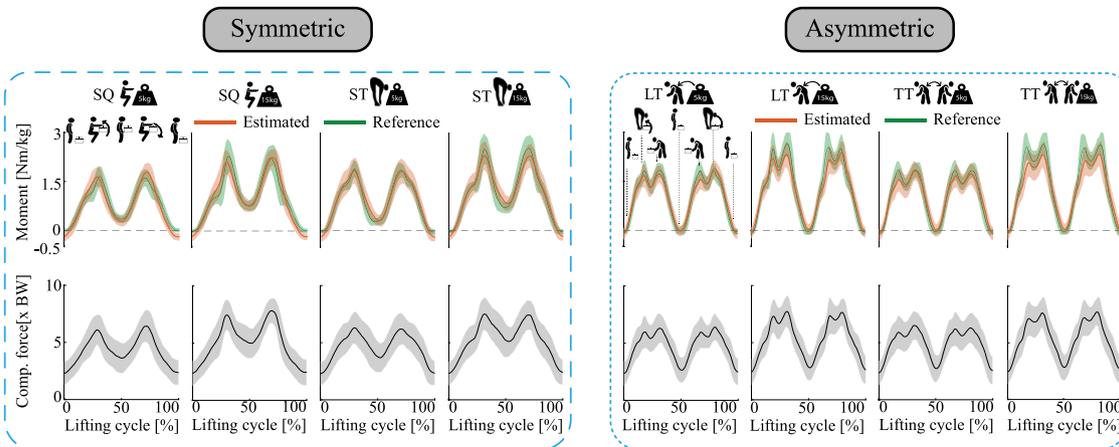
Fig. 3. Mean reference (ID) and estimated (EMG-driven) L5/S1 flexion–extension moments (green and red, respectively) and L5/S1 compression forces (black), averaged across participants. Moments and compression forces are normalized to body weight (BW). Columns represent all experimental conditions, from left to right: squat (SQ 5 and 15 kg), stoop (ST 5 and 15 kg), lift-transfer (LT 5 and 15 kg) and twist-transfer (TT 5 and 15 kg). Shaded areas correspond to $\pm$ 1 standard deviation. (For interpretation of the references to color in this figure legend, the reader is referred to the web version of this article.)
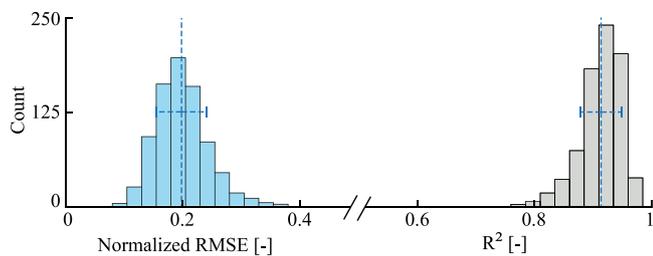
Fig. 4. Histogram depicting the distribution of $RMSE_{RMS}$ (root mean squared error normalized to root mean square of the reference moment) and coefficient of determination, R^2, in blue and gray, respectively, for all participants, conditions and repetitions. Vertical dashed lines indicate the mean value and horizontal error bars ± 1 standard deviation. (For interpretation of the references to color in this figure legend, the reader is referred to the web version of this article.)

moments, and between 1.65 and 2.53 Nm/kg, for reference moments (Table 2). During asymmetric conditions, moments peaked on four occasions, since there were two lift-offs and two box placements. Maximum peaks ranged from 1.82 to 2.38 Nm/kg (estimated moments), and from 1.84 to 2.66 Nm/kg (reference moments).

L5/S1 joint compression forces showed analogous patterns to those of joint moments (Fig. 3). Compression forces exhibited peak magnitudes at box lift-off and box placement stages. Unlike joint moments, the lowest mean compression forces were found during stoop conditions, for both 5 and 15 kg weight conditions (Table 2). Across participants and conditions, the lowest compression force peak was found during stoop 5 kg condition (6.3 times of body weight) and the highest, during squat 15 kg (7.83 times of body weight).

3.2. EMG-to-force relation

In a subset of lifting conditions and muscles (green cells in Table 3), statistical analyses revealed that EMG peaks at box-lifting were significantly higher than EMG peaks at box-lowering. However, the associated MTU forces in the same box-lifting and lowering phases showed no significant difference or were higher at lowering (despite EMG decrease). Across all participants, the longissimus thoracis pars lumborum muscle (LTpL) displayed a variation in EMG during stoop 15 kg condition, which was −19.8%, while the corresponding MTU force variation was −1.0%, indicating reductions of EMG and force at box-lowering relative to lifting values. Nonetheless, for squat 15 kg, EMG decreased by −1.4% and force increased by 1.3% (Fig. 5). Results for all investigated muscles are enclosed in the Supplementary Materials (supplementary figures 1 and 2).

Specifically, results revealed that the occurrence of the aforementioned phenomenon was predominant in conditions involving stooped postures, such as stoop, lift-transfer and twist-transfer (Table 3). For asymmetric liftings, the phenomenon was primarily visible in the muscles located on the opposite side relative to the lifting motion, *e.g.* in trunk right-side muscles when the box was lifted from the left table. Finally, the phenomenon was mainly present in lumbar musculature rather than thoracic (effect found in 10, 9 and 3 occasions for iliocostalis, longissimus thoracis pars lumborum and thoracis, respectively).

For lumbar muscles (iliocostalis and longissimus thoracis pars lumborum) and conditions where concurrent EMG reduction with no MTU force reduction was present, we observed statistically significant linear correlations (ρ range: −0.42 to −0.69, $p < 0.001$), between EMG

Table 3

p-values for statistical tests comparing electromyograms (EMGs) and muscle–tendon unit (MTU) force at box-lifting and lowering instances. Green cells indicate experimental conditions and studied muscles where tests revealed: (1) significant reduction of EMG peak at box-lowering with respect to box-lifting phases and (2) no significant reduction or significant increase of associated MTU force. Red cells indicate conditions where this effect was not present. Experimental conditions include: squat (SQ), stoop (ST), lift-transfer (LT), right twist-transfer (RTT) and left twist-transfer (LTT), see Fig. 1. Statistical significance was accepted with *p* < 0.05. Lifting techniques are squat (SQ), stoop (ST), lift-transfer (LT) and twist-transfer (TT).

		Iliocostalis		Longissimus thoracis pars lumborum		Longissimus thoracis pars thoracis	
		Left	Right	Left	Right	Left	Right
SQ 5 kg	EMG	0.106	0.339	0.388	0.964	0.587	0.022
	Force	0.519	0.642	0.082	0.109	0.283	0.002
SQ 15 kg	EMG	0.203	0.047	0.665	0.100	0.721	0.153
	Force	0.117	0.344	0.240	0.037	0.790	0.050
ST 5 kg	EMG	<0.001	0.003	0.002	0.002	0.035	1.000
	Force	0.415	0.040	0.146	0.003	0.539	0.122
ST 15 kg	EMG	0.003	0.002	0.021	0.003	0.109	0.386
	Force	0.210	0.739	0.664	0.344	0.861	0.310
LT 5 kg	EMG	0.004	0.074	0.005	0.386	0.006	0.258
	Force	0.754	0.021	0.754	0.047	0.445	0.109
LT 15 kg	EMG	0.344	0.508	0.020	0.344	0.109	0.290
	Force	0.028	0.021	0.046	0.021	0.799	0.203
RTT 5 kg	EMG	0.005	0.241	<0.001	0.114	0.021	0.754
	Force	0.407	0.021	0.992	0.021	0.021	0.344
RTT 15 kg	EMG	0.048	0.139	0.059	0.252	0.285	0.754
	Force	0.100	0.002	0.078	0.012	0.508	0.344
LTT 5 kg	EMG	0.034	0.002	0.255	0.002	0.754	0.05
	Force	0.001	0.508	0.023	0.373	0.344	0.447
LTT 15 kg	EMG	0.333	0.019	0.524	0.004	0.575	0.015
	Force	0.324	0.480	0.002	0.676	0.203	0.803
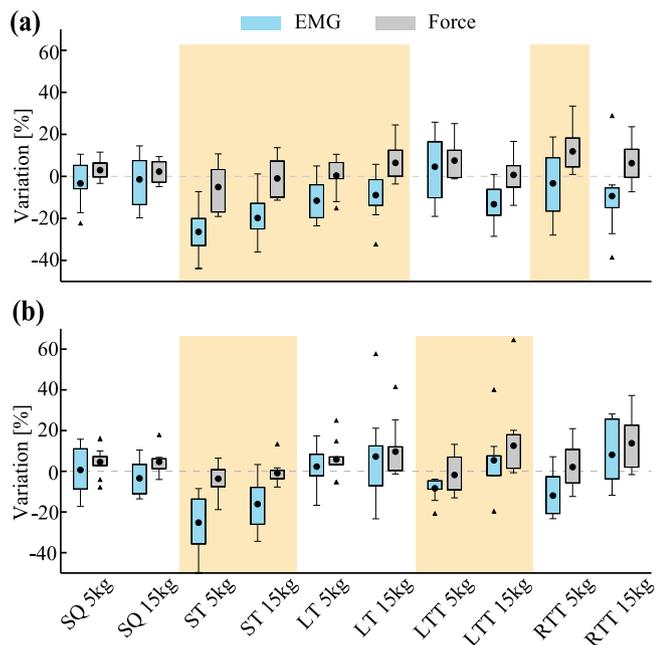
Fig. 5. Percentage of change for EMG and muscle–tendon unit (MTU) force between box-lifting and lowering peaks. Positive and negative values represent an increment or reduction at lowering instances with respect to lifting, respectively. Data is shown for all experimental conditions and a representative muscle: (a) left and (b) right longissimus thoracis pars lumborum. Solid dots and triangles indicate mean values and outliers, respectively. Shaded areas highlight conditions with statistical significant EMG reduction and no significant muscle–tendon force decrease. Lifting techniques are squat (SQ), stoop (ST), lift-transfer (LT) and twist-transfer (TT). For LT, only the asymmetric lifting/lowering motion was considered, *i.e.* movements involving the right table. For TT, we consider two scenarios: lifting and lowering the box when it was placed on the left/right table (LTT and RTT, respectively), see Fig. 1. (For interpretation of the references to color in this figure legend, the reader is referred to the web version of this article.)

Table 4

Pearson correlation coefficients (ρ) for the relationship between percent change of electromyography, EMG, (at box-lowering peaks with respect to lifting) and the percent of change in muscle–tendon unit (MTU) forces derived from force–velocity and force–length relationships. Data is shown for individual, lumbar, thoracic and all muscles and for all experimental conditions where concurrent EMG reduction and no MTU force reduction was observed (termed as "effect"), or not ("no effect").

		Force–velocity		Force–length	
		Effect	No effect	Effect	No effect
Iliocostalis	Left	-0.42	-0.15	-0.07	-0.25
	Right	-0.45	-0.04	0.23	-0.34
Longissimus thoracis pars lumborum	Left	-0.59	0.13	0.34	-0.07
	Right	-0.69	0.10	0.46	0.22
Longissimus thoracis pars thoracis	Left	-0.22	0.04	-0.24	-0.06
	Right	-0.08	-0.12	0.07	-0.06
Lumbar		-0.42	-0.10	0.06	-0.22
Thoracic		0.09	-0.06	-0.10	-0.06
All muscles		-0.36	-0.08	0.05	-0.17

and FV-dependent forces (Table 4 and Fig. 6). Nonetheless, in thoracic muscles we did not find statistically significant correlations ($\rho = 0.09$, $p = 0.413$). Correlation values between EMG and FL-dependent forces were low for both, lumbar and thoracic musculature (0.06 and -0.10, respectively, $p > 0.05$), indicating a predominant contribution of FV-dependent force mechanisms. Therefore, preservation of MTU force despite EMG reduction at box-lowering was primarily contributed by velocity-dependent force generation mechanisms where muscles operated eccentrically, *i.e.* underlying positive normalized fiber velocities (reflecting lengthening contraction) with mean values of 0.39 ± 0.37 cm/s across all participants, experimental conditions and lumbar muscles.
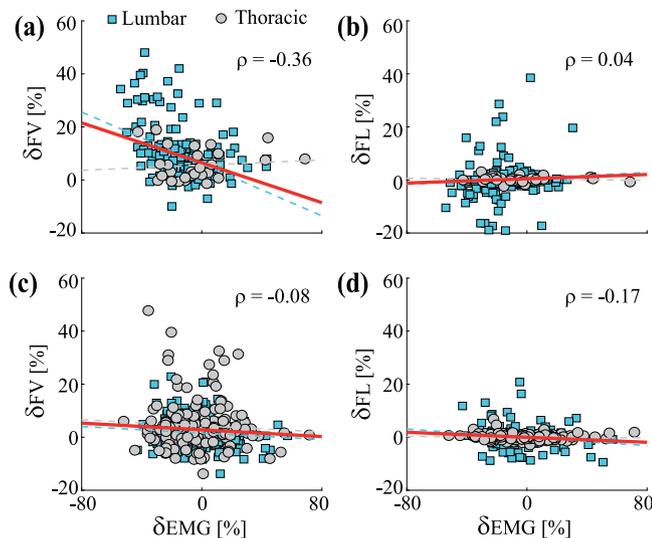
Fig. 6. Variation of electromyographic activity (δEMG) and normalized force–velocity (δFV) and force–length (δFL) dependent forces. Negative values represent a reduction at lowering instances with respect to lifting. For all participants and conditions, (a) and (b) show data with (statistically significant) EMG reduction and no significant muscle–tendon force decrease. (c) and (d) show data for conditions where the aforementioned phenomenon was not present. Dashed blue and gray lines represent regression lines for lumbar and thoracic muscles, while red solid lines is the regression line for all measured muscles. Numeric values indicate the Pearson correlation coefficient for all muscles. (For interpretation of the references to color in this figure legend, the reader is referred to the web version of this article.)

4. Discussion

We developed a subject-specific large-scale EMG-driven musculoskeletal trunk model (238 muscle–tendon units), which yielded accurate estimates of lumbosacral joint moments across a large repertoire of participants, weight as well as symmetric and asymmetric box-lifting conditions. The proposed model also derived realistic lumbosacral compression forces estimates in line with previous literature. For lumbar musculature, our model captured EMG reduction, which did not translate into muscle force decrease, during the lowering phase of the lifting-lowering cycle (Fig. 5). This model-employed strategy underlay the use of eccentric contraction during lowering (Fig. 6). This phenomenon was primarily observed in conditions involving lengthening contractions, *i.e.* symmetric and asymmetric stooped postures. Collectively, our results revealed that our EMG-driven methodology was accurate in reference moment prediction (Figs. 3 and 4), yet robust to different lifting conditions and EMG-to-force non-linearities (Fig. 5). This is a central requirement for the translation of EMG-driven model-based techniques for assistive technologies in real-world scenarios.

Reference peak moments when stooping were always higher than when squat, both for 5 and 15 kg conditions (Table 2), results in line with previous research (Faber et al., 2009; Kingma et al., 2006). While our EMG-driven approach estimated this trend for 5 kg condition, the magnitude of estimated moments for stoop 15 kg was slightly lower than squat 15 kg (2.30 and 2.33 Nm/kg, respectively). Despite moment underestimation during stooping with 15 kg, a quantitative comparison of our model estimates with respect to gold standard (ID) showed, for a total of 10 participants, a high correlation: mean R^2 (range: 0.88–0.94) and $RMSE_{RMS}$ ranging from 17 to 22% of the reference moment. This suggests the possibility of establishing a single EMG-driven model per individual, capable of estimating accurate lumbosacral flexion–extension moments under symmetric, asymmetric and weight conditions.

Compared with 5 kg weight conditions, lumbosacral extension moments generated during 15 kg conditions were substantially higher. In

15 kg weight conditions, peak moments were on average 50 Nm higher than for 5 kg conditions. Previous research showed that symmetrically lifting 7 and 12 kg boxes creates a difference of roughly 20 Nm in L5/S1 flexion–extension moments (Kim and Zhang, 2017). These values suggest that our model presents a sensitivity to weight similar to that of previously validated methodologies.

Our results indicated that compression forces in the lumbosacral joint rose as high as 7.8 times body weight (roughly 5500 N) in both symmetric and asymmetric lifting conditions, for 15 kg weights. *In vivo* measurement of intervertebral joint loads poses a challenge due to the invasiveness of current methodologies, *e.g.* intradiscal pressure sensors (Takahashi et al., 2006). Hence, a direct validation of our compression forces estimates was unfeasible. Nevertheless, the magnitude of our estimates was in line with previous literature. In earlier research, a previously validated EMG-driven model (van Dieën and Kingma, 2005) was used to estimate compression forces while lifting loads using squat and stoop lifting techniques (Faber et al., 2009). Peak compression forces appeared during lift-off with mean values around 5500 N, for 20 kg weights. In Koopman et al. (2020a), compression forces peaks reached 7 times participants body weight when lifting 10 kg boxes. Static optimization methods have also found compression force peaks of 5000 N when asymmetrically lifting 12 kg boxes (Kim and Zhang, 2017).

During symmetric or asymmetric stooped postures, we found EMGs to decrease during box-lowering (eccentric phase) with respect to lifting (concentric). While this phenomenon was not well reflected in thoracic musculature, it was predominant in iliocostalis and longissimus thoracis pars lumborum muscles (Table 3). Similarly, previous studies reported greater EMGs in the concentric phase of liftings, for the lumbar erector spinae (Nijem et al., 2016; Bazrgari et al., 2007). Nonetheless, MTU force (and lumbosacral joint moments) estimates did not show an analogous reduction during eccentric lifting.

In conditions with significant EMG reduction and no MTU force decrease, correlation values linked EMG reduction to an increase of force generated due to the force–velocity relationship. Additionally, weak correlations were found between changes in EMG and forces from the force–length relationship. These results suggest that our model exploited primarily force–velocity dependent mechanisms during eccentric contraction as the main strategy of force enhancement for counteracting decreased muscle activation. While the aforementioned model-employed strategy was significant for lumbar muscles, a similar trend was not found in thoracic muscles, which may be explained by the fact that during stooped postures, lumbar musculature undergoes higher stretch (and stretch velocities) than thoracic. Our model-based findings will be corroborated in future research by combining ultrasound techniques with muscle force measurements.

Our results suggest that the proposed framework was capable of accounting for the non-linear EMG-to-force relationship occurring during box-lowering: peak-EMG reduction and force preservation due to eccentric muscle operation. Although our model findings need to be validated at muscle level in future work, the ability of the proposed model to exploit velocity-dependent force-generation mechanisms to compensate for EMG reduction has crucial implications for robust myoelectric control of assistive devices. Current model-free myoelectric control techniques are challenged in dealing with EMG-to-force non-linearities, *e.g.* neural networks (Aghazadeh et al., 2020; Hou et al., 2007) mapping EMG amplitude into joint kinematics are challenged in generalizing to large sets of movements (Fleming et al., 2021). Hence, the use of model-based techniques may be a viable solution to take into direct account enhanced muscle force-generation capacity during eccentric contractions (Duchateau and Enoka, 2016), (despite associated EMG amplitude reduction), predominant in weight lifting.

A main limitation of the present study consists of the lack of direct validity of our lumbo-sacral compression force estimates. However, our model-derived estimates fell in line with those presented in previous research based on EMG-driven (Koopman et al., 2020a; Faber et al., 2009)

and static optimization-based methodologies (Kim and Zhang, 2017). Additionally, the lack of diverse characteristics among participants is a limitation, which may hamper the extrapolation of our results to a more diverse set of participants. The current use of in-ground force plates and non-wearable motion capture system for lumbar force estimation limits the applicability of our method in out-of-the-lab scenarios. In future studies, we will investigate the use of fully wearable sensors such as inertial measurements units, pressure insoles and zero-wire wearable EMGs for both model calibration and compression force estimation.

The proposed methodology lays the foundations for accurate and robust exoskeleton myoelectric controllers capable of accounting for EMG-to-force non-linearities and estimating realistic lumbar joint forces. This is expected to impact a variety of real-world scenarios such as occupational domains. Furthermore, our framework presents the potential to provide lumbar loading biofeedback in numerous conditions, hence, constituting a tool for rehabilitation and ergonomic applications.

CRediT authorship contribution statement

A. Moya-Esteban: Writing – review & editing, Writing – original draft, Visualization, Validation, Software, Methodology, Investigation, Formal analysis, Data curation, Conceptualization. **H. van der Kooij:** Writing – review & editing, Supervision, Project administration, Funding acquisition, Conceptualization. **M. Sartori:** Writing – review & editing, Supervision, Project administration, Investigation, Funding acquisition, Conceptualization.

Declaration of competing interest

The authors declare that they have no known competing financial interests or personal relationships that could have appeared to influence the work reported in this paper.

Acknowledgments

Appendix A. Supplementary data

Supplementary material related to this article can be found online at https://doi.org/10.1016/j.jbiomech.2022.111307.

References

Aghazadeh, F., Arjmand, N., Nasrabadi, A., 2020. Coupled artificial neural networks to estimate 3D whole-body posture, lumbosacral moments, and spinal loads during load-handling activities. J. Biomech. 102, 109332.

Balagué, F., Mannion, A.F., Pellisé, F., Cedraschi, C., 2012. Non-specific low back pain. Lancet 379 (9814), 482–491. http://dx.doi.org/10.1016/S0140-6736(11)60610-7.

Bazrgari, B., Shirazi-Adl, A., Arjmand, N., 2007. Analysis of squat and stoop dynamic liftings: muscle forces and internal spinal loads. Eur. Spine J. 16 (5), 687–699.

Beaucage-Gauvreau, E., Robertson, W.S., Brandon, S.C., Fraser, R., Freeman, B.J., Graham, R.B., Thewlis, D., Jones, C.F., 2019. Validation of an OpenSim full-body model with detailed lumbar spine for estimating lower lumbar spine loads during symmetric and asymmetric lifting tasks. Comput. Methods Biomech. Biomed. Eng. 1–14. http://dx.doi.org/10.1080/10255842.2018.1564819.

Bosch, T., van Eck, J., Knitel, K., de Looze, M., 2016. The effects of a passive exoskeleton on muscle activity, discomfort and endurance time in forward bending work. Applied Ergon. http://dx.doi.org/10.1016/j.apergo.2015.12.003.

Cholewicki, J., McGill, S.M., Norman, R.W., 1995. Comparison of muscle forces and joint load from an optimization and EMG assisted lumbar spine model: towards development of a hybrid approach. J. Biomech. 28 (3), 321–331.

Coenen, P., Gouttebarge, V., burght, a., Van Dieen, J., Frings-Dresen, M., Beek, A., Burdorf, A., 2014. The effect of lifting during work on low back pain: A health impact assessment based on a meta-analysis. Occup. Environ. Med. 71, http://dx.doi.org/10.1136/oemed-2014-102346.

Coenen, P., Kingma, I., Boot, C.R.L., Twisk, J.W.R., Bongers, P.M., van Dieën, J.H., 2013. Cumulative low back load at work as a risk factor of low back pain: A prospective cohort study. J. Occupat. Rehab. 23 (1), 11–18. http://dx.doi.org/10.1007/s10926-012-9375-z.

De Looze, M.P., Bosch, T., Krause, F., Stadler, K.S., O'sullivan, L.W., 2016. Exoskeletons for industrial application and their potential effects on physical work load. Ergonomics 59 (5), 671–681. http://dx.doi.org/10.1080/00140139.2015.1081988.

Delp, S.L., Anderson, F.C., Arnold, A.S., Loan, P., Habib, A., John, C.T., Guendelman, E., Thelen, D.G., 2007. OpenSim: Open-source software to create and analyze dynamic simulations of movement. IEEE Trans. Biomed. Eng. 54 (11), 1940–1950. http://dx.doi.org/10.1109/TBME.2007.901024.

Duchateau, J., Enoka, R.M., 2016. Neural control of lengthening contractions. J. Exp. Biol. 219 (2), 197–204.

Faber, G.S., Kingma, I., Bakker, A.J., van Dieën, J.H., 2009. Low-back loading in lifting two loads beside the body compared to lifting one load in front of the body. J. Biomech. 42 (1), 35–41. http://dx.doi.org/10.1016/J.JBIOMECH.2008.10.013.

Fleming, A., Stafford, N., Huang, S., Hu, X., Ferris, D.P., Huang, H.H., 2021. Myoelectric control of robotic lower limb prostheses: a review of electromyography interfaces, control paradigms, challenges and future directions. J. Neural Eng..

Gerus, P., Sartori, M., Besier, T.F., Fregly, B.J., Delp, S.L., Banks, S.A., Pandy, M.G., D'Lima, D.D., Lloyd, D.G., 2013. Subject-specific knee joint geometry improves predictions of medial tibiofemoral contact forces. J. Biomech. 46 (16), 2778–2786. http://dx.doi.org/10.1016/j.jbiomech.2013.09.005.

Goffe, W.L., Ferrier, G.D., Rogers, J., 1994. Global optimization of statistical functions with simulated annealing. J. Econometrics 60 (1), 65–99. http://dx.doi.org/10.1016/0304-4076(94)90038-8.

Hara, H., Sankai, Y., 2010. Development of HAL for lumbar support. In: SCIS and ISIS 2010 - Joint 5th International Conference on Soft Computing and Intelligent Systems and 11th International Symposium on Advanced Intelligent Systems. pp. 416–421.

Hou, Y., Zurada, J.M., Karwowski, W., Marras, W.S., Davis, K., 2007. Estimation of the dynamic spinal forces using a recurrent fuzzy neural network. IEEE Trans. Syst. Man Cybern. B 37 (1), 100–109.

Hughes, R.E., Bean, J.C., Chaffin, D.B., 1995. Evaluating the effect of co-contraction in optimization models. J. Biomech. 28 (7), 875–878.

Hughes, R.E., Chaffin, D.B., Lavender, S.A., Andersson, G.B., 1994. Evaluation of muscle force prediction models of the lumbar trunk using surface electromyography. J. Orthopaedic Res, 12 (5), 689–698.

Huysamen, K., de Looze, M., Bosch, T., Ortiz, J., Toxiri, S., O'Sullivan, L.W., 2018. Assessment of an active industrial exoskeleton to aid dynamic lifting and lowering manual handling tasks. Applied Ergon. http://dx.doi.org/10.1016/j.apergo.2017.11.004.

Kim, H.-K., Zhang, Y., 2017. Estimation of lumbar spinal loading and trunk muscle forces during asymmetric lifting tasks: application of whole-body musculoskeletal modelling in OpenSim. Ergonomics 60 (4), 563–576. http://dx.doi.org/10.1080/00140139.2016.1191679.

Kingma, I., Faber, G.S., Bakker, A.J., van Dieën, J.H., 2006. Can low back loading during lifting be reduced by placing one leg beside the object to be lifted? Phys. Ther. 86 (8), 1091–1105. http://dx.doi.org/10.1093/ptj/86.8.1091.

Koopman, A.S., Näf, M., Baltrusch, S.J., Kingma, I., Rodriguez-Guerrero, C., Babič, J., de Looze, M.P., van Dieën, J.H., 2020a. Biomechanical evaluation of a new passive back support exoskeleton. J. Biomech. 105, 109795.

Koopman, A.S., Toxiri, S., Power, V., Kingma, I., van Dieën, J.H., Ortiz, J., de Looze, M.P., 2019. The effect of control strategies for an active back-support exoskeleton on spine loading and kinematics during lifting. J. Biomech. http://dx.doi.org/10.1016/j.jbiomech.2019.04.044.

Lambeek, L.C., Van Tulder, M.W., Swinkels, I.C., Koppes, L.L., Anema, J.R., Van Mechelen, W., 2011. The trend in total cost of back pain in the netherlands in the period 2002 to 2007. Spine 36 (13), 1050–1058. http://dx.doi.org/10.1097/BRS.0b013e3181e70488.

Lloyd, D.G., Besier, T.F., 2003. An EMG-driven musculoskeletal model to estimate muscle forces and knee joint moments in vivo. J. Biomech. 36 (6), 765–776. http://dx.doi.org/10.1016/S0021-9290(03)00010-1.

Marras, W.S., Granata, K.P., 1997. The development of an EMG-assisted model to assess spine loading during whole-body free-dynamic lifting. J. Electromyogra. Kinesiol. 7 (4), 259–268.

McGill, S.M., 1991. Electromyographic activity of the abdominal and low back musculature during the generation of isometric and dynamic axial trunk torque: Implications for lumbar mechanics. J. Orthopaedic Res. 9 (1), 91–103. http://dx.doi.org/10.1002/jor.1100090112.

Moya-Esteban, A., Brouwer, N.P., Tabasi, A., Kooij, H.v.d., Kingma, I., Sartori, M., 2020. Muscle-level analysis of trunk mechanics via musculoskeletal modeling and high-density electromyograms. In: 2020 8th IEEE RAS/EMBS International Conference for Biomedical Robotics and Biomechatronics. BioRob, pp. 1109–1114. http://dx.doi.org/10.1109/BioRob49111.2020.9224325.

Nijem, R.M., Coburn, J.W., Brown, L.E., Lynn, S.K., Ciccone, A.B., 2016. Electromyographic and force plate analysis of the deadlift performed with and without chains. J. Strength Cond. Res. 30 (5), 1177–1182.

Ning, X., Jin, S., Mirka, G.A., 2012. Describing the active region boundary of EMG-assisted biomechanical models of the low back. Clin. Biomech. 27 (5), 422–427.

Ning, X., Zhou, J., Dai, B., Jaridi, M., 2014. The assessment of material handling strategies in dealing with sudden loading: The effects of load handling position on trunk biomechanics. Applied Ergon. 45 (6), 1399–1405. http://dx.doi.org/10.1016/j.apergo.2014.03.008.

Nussbaum, M.A., Chaffin, D.B., 1998. Lumbar muscle force estimation using a subject-invariant 5-parameter EMG-based model. J. Biomech. 31 (7), 667–672.

Pizzolato, C., Lloyd, D.G., Sartori, M., Ceseracciu, E., Besier, T.F., Fregly, B.J., Reggiani, M., 2015. CEINMS: A toolbox to investigate the influence of different neural control solutions on the prediction of muscle excitation and joint moments during dynamic motor tasks. J. Biomech. http://dx.doi.org/10.1016/j.jbiomech.2015.09.021.

Potvin, J., Norman, R., McGill, S., 2004. Mechanically corrected EMG for the continuous estimation of erector spinae muscle loading during repetitive lifting. Eur. J. Appl. Physiol. Occupat. Physiol. 74, 119–132.

Sartori, M., Reggiani, M., Farina, D., Lloyd, D.G., 2012. EMG-driven forward-dynamic estimation of muscle force and joint moment about multiple degrees of freedom in the human lower extremity. PLoS ONE 7 (12), 52618. http://dx.doi.org/10.1371/journal.pone.0052618.

Sparto, P.J., Parnianpour, M., Marras, W.S., Granata, K.P., Reinsel, T.E., Simon, S., 1998. Effect of electromyogram-force relationships and method of gain estimation on the predictions of an electromyogram-driven model of spinal loading. Spine 23 (4), 423–429.

Takahashi, I., Kikuchi, S.-i., Sato, K., Sato, N., 2006. Mechanical load of the lumbar spine during forward bending motion of the trunk–a biomechanical study. Spine 31 (1), 18–23. http://dx.doi.org/10.1097/01.brs.0000192636.69129.fb.

van Dieën, J.H., Kingma, I., 1999. Total trunk muscle force and spinal compression are lower in asymmetric moments as compared to pure extension moments. J. Biomech. 32 (7), 681–687.

van Dieën, J., Kingma, I., 2005. Effects of antagonistic co-contraction on differences between electromyography based and optimization based estimates of spinal forces. Ergonomics 48 (4), 411–426. http://dx.doi.org/10.1080/00140130512331332918.

von Arx, M., Liechti, M., Connolly, L., Bangerter, C., Meier, M.L., Schmid, S., 2021. From stoop to squat: A comprehensive analysis of lumbar loading among different lifting styles. Front. Bioeng. Biotechnol. 9.